Applied Catalysis B: Environmental 313 (2022) 121446

Contents lists available at ScienceDirect

Applied Catalysis B: Environmental

journal homepage: www.elsevier.com/locate/apcatb

Ni-Fe alloying enhances the efficiency of the maltose hydrogenation process: The role of surface species and kinetic study

Achraf Sadier, Sébastien Paul, Eric Marceau, Robert Wojcieszak *

Univ. Lille, CNRS, Centrale Lille, Univ. Artois, UMR 8181 – UCCS – Unité de Catalyse et Chimie du Solide, F-59000 Lille, France

ARTICLE INFO

Keywords:
Maltose
Hydrogenation
Bimetallic nanoparticles
Iron
Kinetic study

ABSTRACT

Unlike the conversion of monosaccharides to the corresponding polyols, the production of maltitol by hydrogenation of maltose has been seldom investigated in the literature, despite its industrial importance. Monometallic Ni catalysts are known for their lack of stability, and the objective of the present paper is to determine through a kinetic study, to what extent a Ni-Fe/SiO_2 bimetallic catalyst would outperform a Ni/SiO_2 catalyst in the aqueous phase hydrogenation of maltose, as they have been reported to do for monosaccharides. The effect of reaction parameters (T = 80–150 °C, P_{H2} = 20–40 bar, maltose mass fraction in water = 4.4–17.5 wt%) on activity, selectivity, and stability was examined. In all cases, maltitol was the major product, with a carbon balance higher than 98%, but maltose hydrolysis to glucose occurred in the upper range of temperature. In order to preserve both the catalyst selectivity and stability, a temperature of 80 °C was selected for the kinetic study. A first order model including an inhibiting term based on maltose concentration could fit the evolution of the conversion of maltose as a function of time. The adsorption constant of maltose and the apparent hydrogenation rate constant for the Ni-Fe catalyst were both larger by a factor 2–3 compared with the Ni catalyst, indicating a stronger interaction of maltose with the Ni-Fe surface. Another major difference was a reaction order of 0.5 with respect to the hydrogen pressure on Ni-Fe/SiO_2 compared with a near zero-order on Ni/SiO_2, stressing significant differences in coverage of the bimetallic surface. The activity of the Ni-Fe catalyst remained constant for three runs of reaction without major structural changes, while the Ni catalyst deactivated by transforming to a phyllosilicate phase. As far as activity, selectivity and stability are concerned; Ni-Fe/SiO_2 appeared as a better suited catalyst than Ni/SiO_2 for the aqueous phase hydrogenation of maltose at 80 °C, with a more pronounced benefit than formerly reported for xylose on the same catalysts.

1. Introduction

The hydrogenation of saccharides such as glucose, fructose, lactose, xylose and maltose to their corresponding polyols are important processes in the food and pharmaceutical industry [1–5]. In particular, several million tons of maltose are annually produced worldwide through the enzymatic hydrolysis of biomass feedstocks, in particular starch, [6–8] and the hydrogenation of maltose (Scheme 1) is a straightforward method for the production of maltitol, [9] which is used as a potential sugar substitute and as an intermediate for pharmaceutical production [10,11]. However, the selective production of maltitol is challenging because the glycosidic bond can be easily hydrolyzed to glucose which is further hydrogenated to sorbitol [12]. The hydrolysis of maltitol can also lead to the formation of a mixture of sorbitol and glucose, the latter being rapidly hydrogenated into sorbitol. Finally glucose can be isomerized to fructose which was not detected under our reaction conditions.

Hydrogenation processes are interesting strategy for biomass valorization especially using water as a solvent. Main advantages are linked to the nontoxicity of water, facility of post-test separation and high biobased substrates dissolvability in water. Water considered as one of the most promising and economically competitive “green solvents” can also participate in the reaction through hydrogen bonds formation or as hydrogen donor [13,14]. However, the hydrothermal stability of heterogenous catalysts in hot water is one of the limiting factors of aqueous phase hydrogenations [15]. Severe reaction conditions such as high temperatures and hydrogen pressures are generally needed to reach high product yields especially when working with non-noble metals [16]. Various heterogeneous catalysts, based on non-noble metals such us Ni, Cu, and Fe have been studied in sugar hydrogenation [17–21].

* Corresponding author.
E-mail address: robert.wojcieszak@univ-lille.fr (R. Wojcieszak).

https://doi.org/10.1016/j.apcatb.2022.121446
Received 24 January 2022; Received in revised form 19 April 2022; Accepted 22 April 2022
Available online 26 April 2022

Nickel -based catalysts are generally favored because of their excellent activities and low cost. However, the Ni catalysts in water exhibit usually high deactivation rate due to metal leaching, metal particle sintering, and/or active site poisoning by adsorption of byproducts formed during side reactions. Thus, a drastic enhancement in the catalytic activity and stability of non-noble catalysts is still a challenge.

The hydrogenation of maltose to maltitol has been much less studied in the academic literature than that of monosaccharides. As is often the case for the reductive transformation of biosourced molecules, Ru-based catalysts are both very active and selective in the catalytic hydrogenation of maltose in aqueous solutions (selectivity to maltitol > 95% at full conversion, for mass fractions of maltose in water = 4–40 wt%, T = 90–140 °C, $P(H_2)$ = 20–70 bar) [9,17,22–26]. But the cost and availability of noble metals are the major drawbacks for their industrial application and, to date, Raney® Ni is the most common benchmark catalyst for this reaction [27–30]. A selectivity to maltitol of 85–99% was reported to be achieved at high conversion in a range of reaction temperature of 80–170 °C, under 28–70 bar of H_2, using concentrated aqueous solutions of maltose (mass fractions = 20–50 wt%). However, Raney® Ni deactivates under reaction by leaching of nickel and by deposition of by-products formed by side reactions [10,31–33].

A common way to tackle with problems of catalytic performance and stability is to associate two elements in the catalytic phase. Up to now, this strategy has not been implemented to a large extent for maltose hydrogenation. A recent system based on a Ni−P nanoalloy supported on basic solids has been studied [34–36]. Ni-P/HT and Ni-P/mSiO_2 −NH_2&CH_3 (HT: hydrotalcite: $Mg_6Al_2CO_3(OH)_{16}.4(H_2O)$, m$SiO_2$ −NH_2&CH_3: functionalized mesoporous silica) were investigated in a 10–50 wt% maltose aqueous solution, at 60–150 °C, under 20–50 bar of H_2 [34–36]. Under optimum conditions, selectivity to maltitol of 90–95% was achieved at almost full conversion. Ni-P/HT retained its activity and selectivity toward maltitol (95% at 95% conversion) during four runs of reactions [34]. Ni-P/SiO_2-NH_2 displayed a good stability in the aqueous phase hydrogenation of maltose after six runs of reactions [36].

In a few works, the advantages of adding iron to Ni for the aqueous phase hydrogenation of monosaccharides (xylose and glucose) have been reported and it was demonstrated that both the activity and stability of the catalysts were enhanced by Fe addition [37–39]. The objective of the present paper is to determine for the first time, through a kinetic study, to what extent a Ni-Fe/SiO_2 bimetallic catalyst would outperform a Ni/SiO_2 catalyst in the aqueous phase hydrogenation of maltose, as they have been reported to do for monosaccharides [37–39]. The effect of reaction parameters (e.g., temperature, maltose concentration, hydrogen pressure) on catalytic activity, selectivity, and stability will be examined. In-depth advanced characterization (Low-energy ion scattering - LEIS, High resolution transmission electron microscopy - HRTEM, Mössbauer spectroscopy) of studied materials was performed and it is presented in details in our previous works on these catalysts [37,40].

2. Experimental section

Ni_{100}/SiO_2 and $Ni_{62}Fe_{38}/SiO_2$ catalysts were prepared by deposition-precipitation with urea according to the procedure detailed in our previous work [37,40]. For $Ni_{62}Fe_{38}/SiO_2$, the Ni and Fe loadings were 26 and 16 wt%, respectively. *Fcc* Ni-Fe alloyed nanoparticles were observed by XRD and TEM analysis. The bimetallic particles were homogeneous in size (average size: 5.4 nm; standard deviation: 1.3 nm) and composition (standard deviation of composition: 8 Fe at%). Ni_{100}/SiO_2 exhibited a 40 wt% loading of Ni. *Fcc* Ni was observed by XRD analysis with 5.4 nm as an average particle size.

The elemental analysis of Ni, Fe, and Si in solutions was done by ICP-OES (Inductively Coupled Plasma Optical Emission Spectrometry) analysis by using Agilent 720-ES ICP-OES equipment combined with Vulcan 42 S automated digestion system. Powder X-ray diffraction patterns (XRD) of the samples were recorded in ambient conditions using a Bruker AXS D8 Advance diffractometer equipped with a nickel filter, a copper tube (λKα (Cu) = 1.54184 Å) and a multi-channel fast detector. Samples were scanned at 0.014° s^{-1} over the range $5 \leq 2\theta \leq 80$ °.

The hydrogenation of maltose (Alfa Aesar, 96%) was carried out in a 30 mL batch Hastelloy Parr autoclave. In a typical reaction, a substrate aqueous solution of 24 mL (8.8 wt% of maltose, corresponding to concentrations of 95 g L^{-1} and 0.26 mol L^{-1}) and 108 mg of catalyst were loaded into the reactor. After purging the reactor 3 times with H_2, 20 bar H_2 was added and the system was heated to the reaction temperature (T = 80–150 °C) with a stirring rate of 600 rpm. The effect of mass of catalysts up to 108 mg was studied to check the absence of diffusion limitation. At the end of the reaction, pressure was removed, the reactor was cooled, and the catalyst was collected by centrifugation. Blank tests were performed in which no conversion of maltose was observed. Maltose, maltitol, glucose, and sorbitol were analyzed by High Performance Liquid Chromatography (HPLC,Waters 2410 RJ) equipped

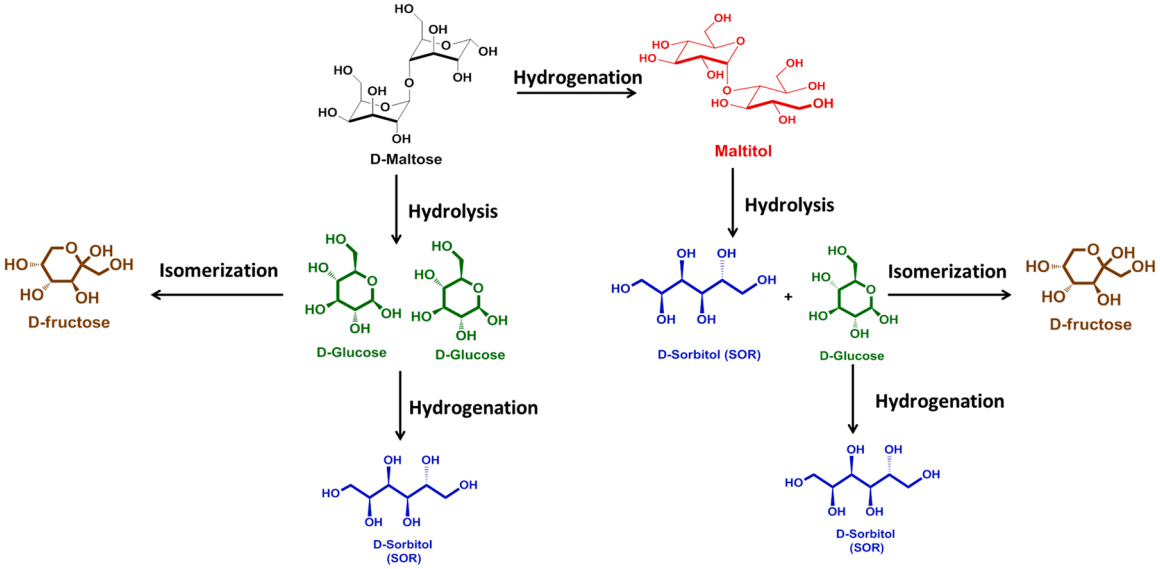

Scheme 1. Reaction pathways from the hydrogenation of maltose.

with RI and UV detectors and a Rezex ROA–organic Acid H^+ column (Ø 7.8 mm × 300 mm) at 25 °C. Diluted H_2SO_4 (5 mM, 0.5 mL/min) was used as a mobile phase. The products were identified by their retention times compared to available standards and the response factors were determined experimentally for these commercial products. The hydrogenation products of maltose are well separated by the HPLC column as shown on a typical chromatogram (Fig. S1).

The conversion of maltose at time t was calculated from Eq. (1):

$$Conversion_t(\%) = \frac{C_0^{maltose} - C_t^{maltose}}{C_0^{maltose}} \times 100 \quad (1)$$

where $C_0^{maltosee}$ is the initial concentration of maltose (in mol L^{-1}) and $C_t^{maltose}$ is the concentration of maltose at time t (in mol L^{-1}). The carbon selectivity S_t^i to a desired product was calculated using Eq. (2):

$$S_t^i(\%) = \frac{C_t^{product\ \ i} \times \ n_C^{product\ i}}{(C_0^{maltose} - C_t^{maltosee}) \times 12} \times 100 \quad (2)$$

in which $C_t^{product\ i}$ is the concentration of product i at time t (in mol L^{-1}); $n_C^{product\ i}$ is the number of carbon atoms in the product i.

The calculated TOC (Total Organic Carbon) at time t is determined by the sum of the carbon concentrations of all compounds quantified by HPLC according to Eq. (3).

$$TOC \quad calculated_t(\quad g \quad L^{-1}) = M_C\left[\left(\sum_i^n n_{carbon}^i \times C_t^i\right)\right] \quad (3)$$

where M_C is the molar mass of carbon $= 12$ g mol^{-1}; n_{carbon}^i is the number of carbon atoms in the compound i; C_t^i is the concentration of compound i at time t (in mol L^{-1}).

The carbon balance (CB) at time t is calculated according to Eq. (4).

$$\text{Carbon balance(CB)} = \frac{C_t^{maltose} + C_t^{maltitol} + C_t^{glucose} + C_t^{sorbitol}}{C_0^{maltose}} \times 100 \quad (4)$$

Where $C_0^{maltose}$ is initial concentration of maltose (in mol L^{-1}), $C_t^{maltose}$, $C_t^{maltitol}$, $C_t^{glucose}$, and $C_t^{sorbitol}$, are the concentrations of maltose, maltitol, glucose and sorbitol, respectively, at time t (in mol L^{-1}).

At the end of the tests, the aqueous solution was analyzed by ICP to detect the leaching of metals expressed in ppm.

3. Results and discussion

3.1. Definition of benchmark conditions with Ni_{100}/SiO_2

The hydrogenation of maltose (concentration: 0.26 mol L^{-1}) was first carried out at 150 °C under 20 bar H_2 in the presence of 108 mg of the monometallic Ni_{100}/SiO_2 catalyst. The evolution of the concentration of maltose and of the reaction products is presented as a function of time in Fig. 1. A conversion of 92% was attained after 160 min. Maltitol was the main product (70% selectivity). It appeared at the initial stage of the reaction and its concentration reached 0.16 mol L^{-1} at 160 min. Side-products (sorbitol and glucose,) were detected after 45 min and their concentration increased to a maximum of 0.11 and 0.05 mol L^{-1}, respectively, at the end of the test. Finally, the calculated carbon balance obtained at the end of the reaction was 98%, indicating that all the products formed in the aqueous phase were detected by HPLC.

3.2. Determination of the reaction parameters: effect of temperature, and metal leaching

The effect of the reaction temperature was then studied over the range 80–150 °C under 20 bar H_2 in the presence of 108 mg of the Ni_{100}/SiO_2 and $Ni_{62}Fe_{38}/SiO_2$ catalysts. The temporal evolution of maltose concentration as a function of temperature is shown in Fig. 2. At

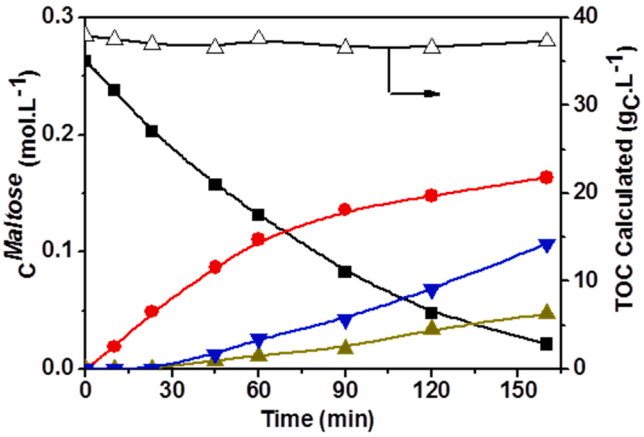

Fig. 1. Temporal evolution of product concentrations during the hydrogenation of maltose: (■) Maltose; (•) Maltitol; (▲) Glucose; (▼) Sorbitol; (△) Calculated carbon balance: Reaction conditions: maltose 0.26 mol L^{-1}, V = 24 mL, 20 bar H_2, 150 °C, 108 mg Ni_{100}/SiO_2, $n_{Maltose}/n_{Ni} = 9.8$.

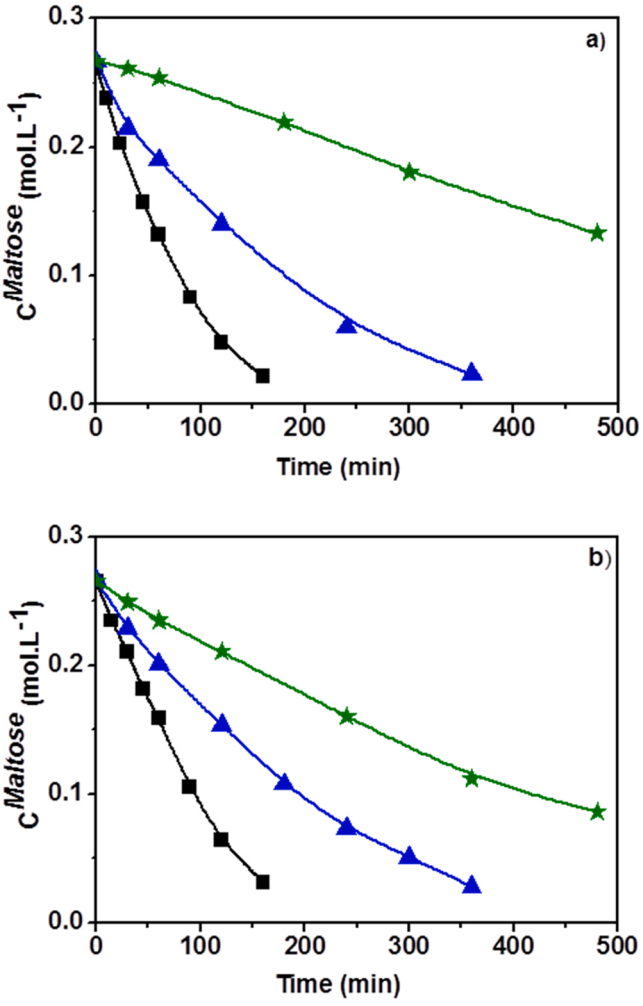

Fig. 2. Effect of reaction temperature on temporal evolution of maltose concentration over a) Ni_{100}/SiO_2, b) $Ni_{62}Fe_{38}/SiO_2$ catalysts: (■) 150 °C; (▲) 100 °C; (*) 80 °C. Reaction conditions: maltose 0.26 mol L^{-1}, V = 24 mL, 20 bar H_2, 108 mg catalyst, $n_{maltose}/n_{Ni} = 9.8$, $n_{maltose}/n_{Ni\ +\ Fe} = 10.0$.

80 °C, a 68% conversion was achieved after 480 min over $Ni_{62}Fe_{38}/SiO_2$, whereas the maltose conversion was limited to 50% using Ni_{100}/SiO_2. As expected, the conversion increased when the temperature increased. The normalized catalytic activity per g of Ni at different temperatures was given in Table S1.

It can be noted that the hydrogenation of maltose in this temperature range was noticeably less rapid than that of xylose hydrogenation [37]. The carbon balance was higher than 98% for both catalysts in the whole temperature range. For preliminary analysis, a pseudo-first order kinetics with respect to maltose was obtained from the plot of ln $(C_0^{maltose}/C_t^{maltose})$ versus time (Fig. S2), in line with former simplified models applied to xylose hydrogenation [41,42]. Table S2 presents the values of the first-order apparent rate constants (k_{app}). The Ni-Fe catalyst exhibited a higher value of k_{app} at 80 °C, but as temperature increased the gap narrowed and at 150 °C the Ni catalyst was the more active of the two.

An important point to consider is selectivity. As temperature decreased from 150° to 80°C, the formation of side-products (glucose and sorbitol, Scheme 1) decreased to a negligible level, as can be seen in the 20–60% conversion range for all the experiments. At 80 °C the reaction was almost 100% selective to maltitol (Fig. S3). It was verified that with either catalyst, maltitol was not hydrolyzed in these reaction conditions. This means that the formation of glucose took place via the competing hydrolysis of maltose, a minor pathway favored with the Ni catalyst. Sorbitol was thus produced by the hydrogenation of glucose issued from the hydrolysis of maltose. It can be assumed that unreduced metal ions acting as Lewis acidic sites (in this case, presumably, unreduced Ni^{2+} ions) catalyze the hydrolysis of maltose, as they were found to account for the etherification of furfuryl alcohol in the presence of the same catalysts [40].

The leaching of metals measured by ICP analysis of the liquid solution recovered at the end of the test is presented as a function of temperature in Fig. 3. The right-hand Y-axis of the graph corresponds to % leaching of Si from catalyst (blue circles). The % leaching of Ni and Si released from Ni_{100}/SiO_2 significantly decreased from 1.5% and 15.3%, to 0.6% and 6.6%, respectively, as the reaction temperature decreased from 150° to 80°C. Using Ni_{100}/SiO_2 at 150 °C is thus beneficial in terms of kinetics, but detrimental in terms of leaching. The same trend was observed for Ni, Fe and Si in the presence of $Ni_{62}Fe_{38}/SiO_2$, with a very low % leaching of the three elements at 80 °C.

Despite the lower reaction rate, a temperature of 80 °C was accordingly chosen for a kinetic study in order to avoid the effect of the side-reaction of maltose hydrolysis, and to limit the leaching of the metals. It was verified for the two catalysts at 80 °C that a linear relationship was obtained between the initial reaction rate of the reaction and the mass of catalysts up to 108 mg, confirming the existence of a kinetic regime without mass transfer limitation (Fig. S4).

3.3. Effect of maltose concentration and hydrogen pressure at 80 °C

The maltose concentration (4.4–17.5 wt%) was varied over the range 0.13–0.58 mol.L^{-1}, while the reaction temperature was set to 80 °C, and the H_2 pressure to 20 bar. A constant volume of solution was used (24 mL) and the concentration was changed by adjusting the mass of maltose.

Fig. 4 presents the temporal evolution of maltose concentration (symbols represent the experimental points and curves the model detailed below). The selectivity toward maltitol was in all cases higher than 98%, with a carbon balance higher than 98%. The $Ni_{62}Fe_{38}/SiO_2$ catalyst exhibited a higher activity than the Ni_{100}/SiO_2 catalyst over the whole range of concentration tested.

The same kinetic model as the one used in our previous work on the selective hydrogenation of xylose to xylitol (Eq. (5)) [37] was applied to these measurements.

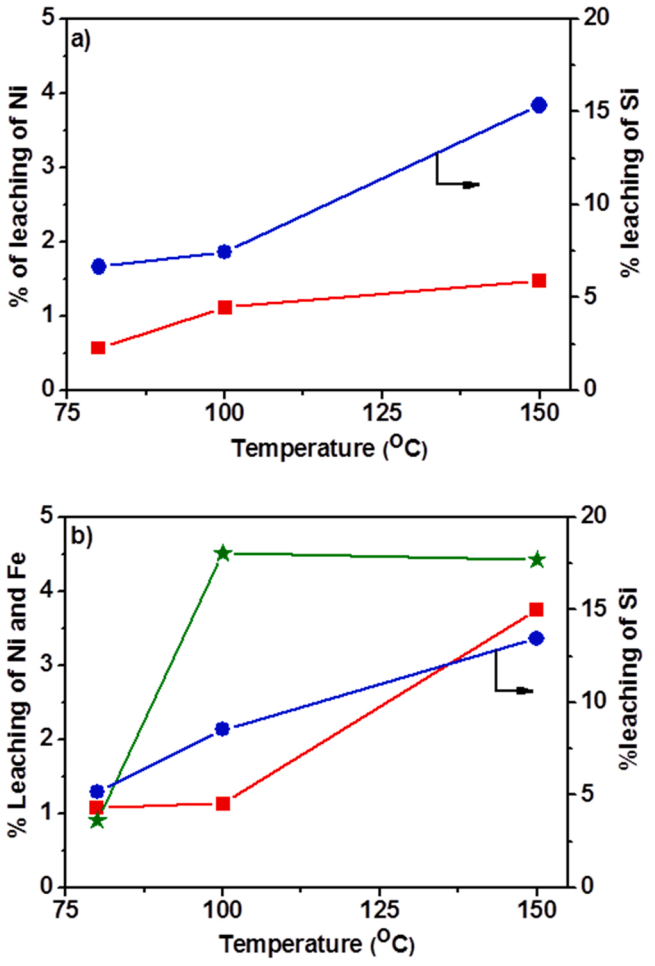

Fig. 3. Effect of reaction temperature on metal leaching over a) Ni_{100}/SiO_2, b) $Ni_{62}Fe_{38}/SiO_2$ catalysts at the end of the reaction. (■) Ni; (*) Fe; (•) Si. Reaction conditions: Reaction conditions: maltose 0.26 mol L^{-1}, V = 24 mL, 20 bar H_2, 108 mg catalyst, $n_{maltose}/n_{Ni} = 9.8$, $n_{maltose}/n_{Ni + Fe} = 10.0$.

$$\text{rate } r = \frac{k \times C^{maltose}}{1 + K \times C^{maltose}} \quad (5)$$

This first-order model supposes a Langmuir-type adsorption of maltose onto the catalyst, described by the constant K in the inhibition term of Eq. (1). A detailed procedure of the inclusion of hydrogen pressure in the rate constant should be provided in the Supplementary Material (p. S7). The values at 80 °C of k, the apparent rate constant in which P_{H2} is included, and K (the adsorption constant of maltose) are given in Table 1 for the two catalysts. Independent refinements of each curve led to consistent results (details can be found in the Supplementary Material, p. S8, Fig. S5) and to a relative error margin of maximum 16%.

The value of the apparent rate constant k for the bimetallic catalyst is larger by a factor 2.7 compared with the monometallic catalyst, whereas the gain was less than a factor 2 for xylose hydrogenation (Table 1). The benefit of using the bimetallic catalyst for maltose hydrogenation at 80 °C thus appears clearly. However, the rate constants for maltose hydrogenation are lower by a factor 5–6 compared with xylose. Such a strong difference is consistent with that reported with a Ru/C catalyst in the selective hydrogenation of maltose vs. monosaccharide sugars [43]. At 120 °C under 60 bar H_2, a 100% conversion was achieved after 50 and 90 min, respectively, for the hydrogenation of 9 wt% L-arabinose and L-rhamnose, while 180 min were needed to complete the hydrogenation of D-maltose.

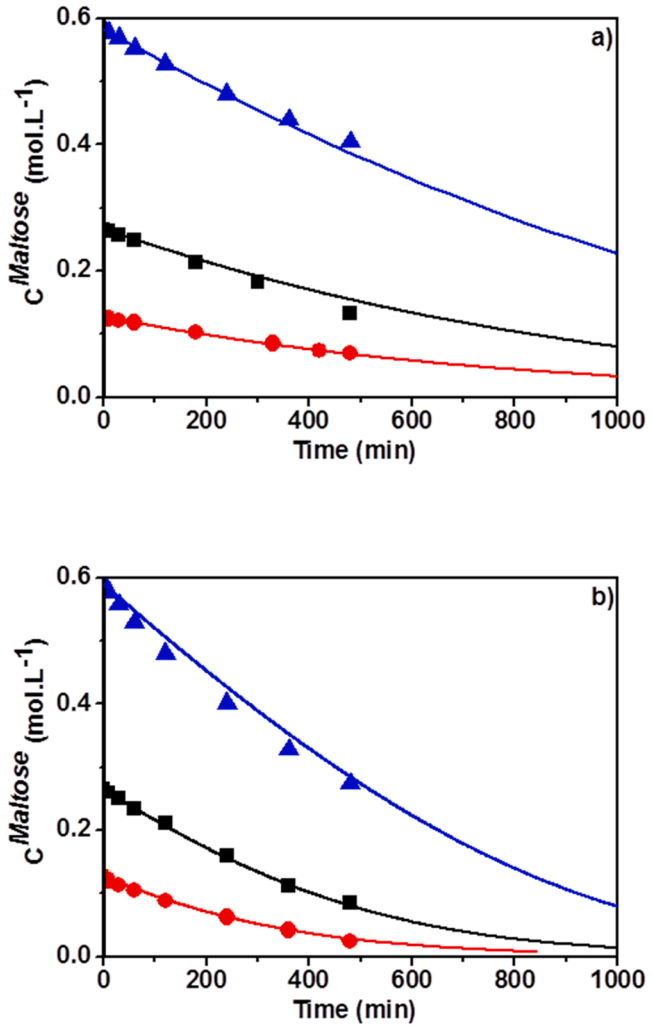

Fig. 4. Evolution of maltose concentration as a function of time and initial maltose concentration over a) Ni_{100}/SiO_2 and b) $Ni_{62}Fe_{38}/SiO_2$ catalysts: (•) 4.4 wt%; (■) 8.8 wt%; (▲) 17.5 wt%. Reaction conditions: 20 bar H_2, 80 °C, 108 mg catalyst. Curves are calculated using the model based on Eq. (2), see Supp Mater.

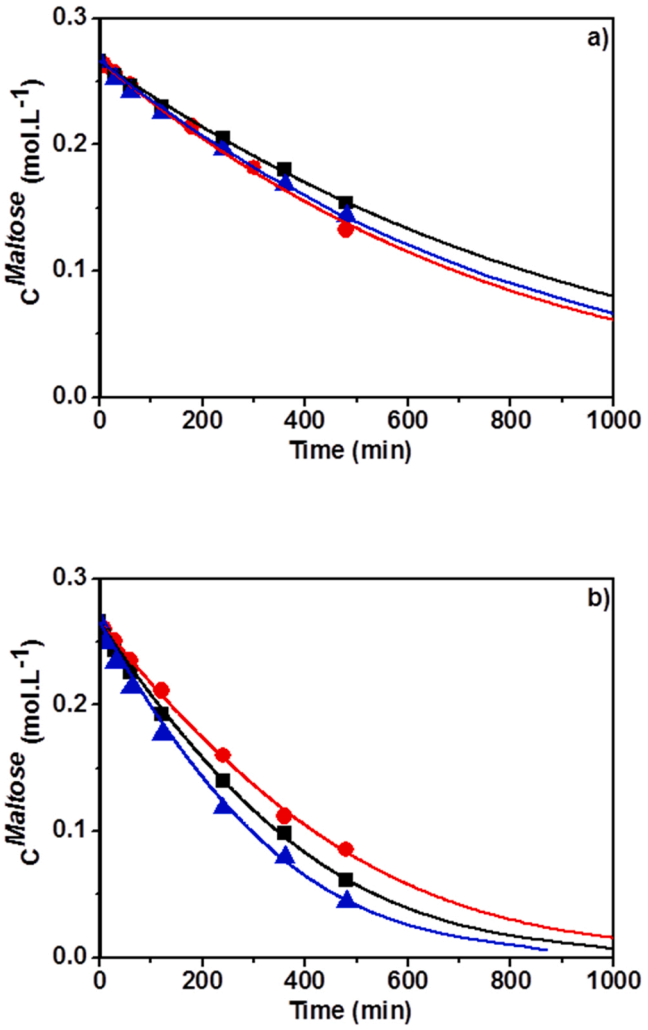

Fig. 5. Evolution of maltose concentration as a function of time and hydrogen pressure over a) Ni_{100}/SiO_2 and b) $Ni_{62}Fe_{38}/SiO_2$ catalysts: (•) 20 bar; (■) 30 bar; (▲) 40 bar. Reaction conditions: maltose 0.26 mol L^{-1}, V = 24 mL, 20 bar H_2, 108 mg catalyst, $n_{maltose}/n_{Ni} = 9.8$, $n_{maltose}/n_{Ni} + n_{Fe} = 10.0$. Curves are calculated using the model based on Eq. (2).

Table 1
Values of rate (k) and adsorption (K) constants for maltose and xylose hydrogenation. Reaction conditions: 20 bar H_2, 80 °C, 108 mg catalyst.

	Maltose		Xylose [37]	
	Ni_{100}/SiO_2	$Ni_{62}Fe_{38}/SiO_2$	Ni_{100}/SiO_2	$Ni_{62}Fe_{38}/SiO_2$
k (min^{-1})	0.0015	0.0040	0.0130	0.0200
K ($L.mol^{-1}$)	1.58	3.90	0.77	2.40

$Ni_{62}Fe_{38}/SiO_2$ also exhibits a larger adsorption constant compared to Ni_{100}/SiO_2 in the hydrogenation of maltose (Table 1). In our model based on a Langmuir-type equation, the adsorption constant K is included in the definition of the apparent rate constant k, and the increase of K can contribute to the increase of the reaction rate constant (k) of the maltose hydrogenation on monometallic and the bimetallic catalysts. It should be noted though that other factors, that cannot be simply determined, also influence the value of k: the value of the kinetic constant of the rate-determining step, which can change if the type of active sites differs, and the number of active sites. This will be discussed below. The oxophilic character of Fe was reported to favor the adsorption of oxygen-containing reactants, compared to Ni surfaces, and this enhancement was also observed for xylose [37]. Unlike what was found for k, the adsorption constants increased by a factor 1.5–2 compared with xylose hydrogenation. Maltose adsorbs more strongly than xylose, but the process of hydrogenation is much slower.

Fig. 5 documents the effect of H_2 pressure (20–40 bar) on conversion at 80 °C, with a 0.26 mol.L^{-1} maltose aqueous solution. Maltitol was the only product obtained with a carbon balance of 98%. The values of k were calculated for each pressure (Table S3) after importing into Eq. (2) the values of K listed in Table 1. It was then supposed that k was a simple function of P_{H2}^{m}. For the Ni_{100}/SiO_2 catalyst, the conversion of maltose did not depend much on the H_2 pressure (Fig. 5a) and the reaction order m was calculated as 0.11 (Fig. S9, from the plot of ln(k) versus ln(P_{H2})). In contrast, in the presence of the $Ni_{62}Fe_{38}/SiO_2$ catalyst, the conversion of maltose increased significantly with the increase of hydrogen pressure (Fig. 5b), and m was found to be equal to 0.50 (Fig. S6). The mechanism of hydrogenation thus seems to differ on the two catalysts, not only with respect to maltose adsorption, but also with respect to hydrogen adsorption and dissociation. An order of 0.5 may correspond to a rate-determining reaction between adsorbed maltose and one hydrogen atom resulting from the dissociative adsorption of H_2, as was observed for xylose hydrogenation [37]. The significantly different reaction orders with respect to H_2, as well as the much lower values of k when comparing maltose hydrogenation with xylose hydrogenation, could be

explained by differences of active sites between the monometallic and the bimetallic catalysts, affecting both hydrogen and the saccharide. As Ni is the metal expected to activate H_2, we suggest that a dilution of Ni domains among Fe surface atoms could account both for the differences of coverage in hydrogen atoms apt to ensure the hydrogenation of the saccharide; and for a lower number of adsorption sites apt to adsorb maltose, a larger molecule compared with xylose, in a favorable configuration for hydrogenation. That the number of adsorption sites is lower for maltose would not be in contradiction with an intrinsically stronger adsorption on the bimetallic surface, as evaluated by K, through the involvement of neighboring oxophilic Fe atoms.

3.4. Stability of Ni_{100}/SiO_2 and $Ni_{62}Fe_{38}/SiO_2$ catalysts in aqueous phase

The recyclability of Ni_{100}/SiO_2 and $Ni_{62}Fe_{38}/SiO_2$ catalysts was examined at 80 °C under 20 bar H_2 during 8 h of reaction (Fig. 6). Before each run, the catalysts were reactivated under H_2 at 400 °C for 2 h. A decrease in the catalytic activity of Ni_{100}/SiO_2 was found after the first run and a conversion of only 8% was retained during the third run. In contrast, no major change was observed for $Ni_{62}Fe_{38}/SiO_2$ (~65–68% conversion). The carbon balance was always higher than 98% and no other product than maltitol was detected. The ICP analysis of the aqueous solutions at the end of each run showed that the leaching of metals (Table S4) was less pronounced for the second and third runs, which did not explain the decrease in catalytic conversion for the Ni_{100}/SiO_2 catalyst. Its deactivation was rather related to its rehydration to a phyllosilicate phase (X-ray diffractograms, Fig. S7), as was observed upon xylose hydrogenation in water [37]. The Fe-rich shell around Ni-Fe nanoparticles would prevent this transformation, and the addition of Fe to Ni would also be beneficial with respect to the catalyst stability.

4. Conclusion

In this kinetic study of the seldom explored aqueous phase hydrogenation of maltose to maltitol, a Ni-Fe/SiO_2 catalyst prepared by deposition-precipitation was found to outperform a reference Ni/SiO_2 catalyst in several respects: a higher activity at 80 °C, a temperature chosen to limit metal leaching and side-reactions of hydrolysis that occur at higher temperatures and compromise the selectivity of the reaction; and a larger structural stability. The evolution of maltose concentration with time could be modeled following a first order kinetic model based on a Langmuir-type adsorption of maltose onto the catalyst. The first-order apparent rate constant and the adsorption constants for the Ni-Fe catalyst were larger by a factor of 2–3 compared with the Ni catalyst. Compared with the hydrogenation of a monosaccharide, xylose, the adsorption constants for maltose were larger by a factor 1.5–2, but the apparent rate constants were much lower, by a factor 5–6. Another major difference between the two catalysts was a reaction order of 0.5 with respect to the hydrogen pressure on Ni-Fe/SiO_2 compared with a near zero-order on Ni/SiO_2. Maltose hydrogenation seems to be driven by an adsorption of maltose very significantly favored on the oxophilic surface of the bimetallic catalyst, but differences in reactants coverage and activation (maltose and hydrogen) should also be invoked to explain the characteristics of the bimetallic catalyst vs. the monometallic catalyst, and of maltose hydrogenation vs. the hydrogenation of monosaccharides.

CRediT authorship contribution statement

Achraf Sadier: Conceptualization, Investigation, Data curation, Writing – original draft. **Sébastian Paul**: Reviewing. **Eric Marceau**: Data curation, Methodology, Supervision, Writing – review & editing, Writing – original draft. **Robert Wojcieszak**: Conceptualization, Visualization, Supervision, Writing – review & editing, Writing – original draft.

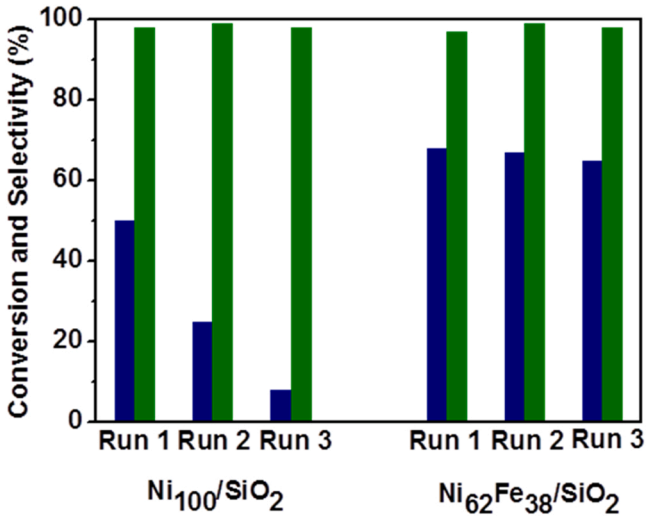

Fig. 6. Catalyst recyclability study. (■) maltose conversion, (■) maltitol selectivity. Reaction conditions: maltose 0.26 mol L^{-1}, V = 24 mL, 20 bar H_2, 80 °C, 108 mg catalyst, reaction time = 8 h, $n_{maltose}/n_{Ni}$ = 9.8, $n_{maltose}/n_{Ni} + n_{Fe}$ = 10.0.

Declaration of Competing Interest

The authors declare that they have no known competing financial interests or personal relationships. that could have appeared to influence the work reported in this paper.

Acknowledgements

The financial support of this work was provided by the French National Research Agency (ANR), through the NobleFreeCat project (ANR-17-CE07-0022). The authors acknowledge the scientific services of the REALCAT platform of UCCS: Joelle Thuriot-Roukos (ICP), Svetlana Heyte (SPR/HPLC). The Chevreul Institute is thanked for its help in the development of this work through the ARCHI-CM project supported by the "Ministère de l'Enseignement Supérieur de la Recherche et de l'Innovation", the region "Hauts-de-France", the ERDF program of the European Union and the "Métropole Européenne de Lille". The REALCAT platform is benefitting from a state subsidy administrated by the French National Research Agency (ANR) within the frame of the 'Future Investments' program (PIA), with the contractual reference 'ANR-11-EQPX-0037'. The European Union, through the ERDF funding administered by the Hauts-de-France Region, has co-financed the platform. Centrale Lille, the CNRS, and University of Lille as well as the Centrale Initiatives Foundation, are thanked for their financial contributions to the acquisition and implementation of the equipment.

Appendix A. Supporting information

Supplementary data associated with this article can be found in the online version at doi:10.1016/j.apcatb.2022.121446.

References

[1] J. Kuusisto, J.-P. Mikkola, M. Sparv, J. Wärnå, H. Heikkilä, R. Perälä, J. Väyrynen, T. Salmi, Ind. Eng. Chem. Res. 45 (2006) 5900–5910.
[2] J. Kuusisto, J.-P. Mikkola, P.P. Casal, H. Karhu, J. Väyrynen, T. Salmi, Chem. Eng. J. 115 (2005) 93–102.
[3] H. Li, P. Yang, D. Chu, H. Li, Appl. Catal. Gen. 325 (2007) 34–40.
[4] J. Kuusisto, M. Tylli, M. Golde, T. Riihimäki, 2014, US 8,816,068.
[5] P. Gallezot, P. Cerino, B. Blanc, G. Fleche, P. Fuertes, J. Catal. 146 (1994) 93–102.
[6] R. Ohba, S. Ueda, Biotechnol. Bioeng. 22 (1980) 2137–2154.
[7] O. Gaouar, C. Aymard, N. Zakhia, G.M. Rios, J. Chem. Technol. Biotechnol. 69 (1997) 367–375.

[8] P.N. Nehete, N.K. Shah, V. Ramamurthy, R.M. Kothari, World J. Microbiol. Biotechnol. 8 (1992) 446–450.
[9] Q. Meng, H. Li, H. Li, J. Phys. Chem. C 112 (2008) 11448–11453.
[10] A. Corma, S. Iborra, A. Velty, Chem. Rev. 107 (2007) 2411–2502.
[11] M. Besson, P. Gallezot, C. Pinel, Chem. Rev. 114 (2014) 1827–1870.
[12] E.M. Sulman, M.E. Grigorev, V. Yu. Doluda, J. Wärnå, V.G. Matveeva, T. Salmi, D. Yu. Murzin, Chem. Eng. J. 282 (2015) 37–44.
[13] M.J. Climent, A. Corma, S. Iborra, Green Chem. 16 (2014) 516–547.
[14] X. Li, L. Zhang, S. Wang, Y. Wu, Front. Chem. 7 (2020) 948.
[15] L. Hu, L. Lin, S. Liu, Ind. Eng. Chem. Res. 53 (2014) 9969–9978.
[16] W.F. Simanullang, H. Itahara, N. Takahashi, S. Kosaka, K. Shimizu, S. Furukawa, Chem. Commun. 55 (2019) 13999–14002.
[17] K. van Gorp, E. Boerman, C.V. Cavenaghi, P.H. Berben, Catal. Today 52 (1999) 349–361.
[18] M.J. Ahmed, B.H. Hameed, J. Taiwan Inst. Chem. Eng. 96 (2019) 341–352.
[19] A. Romero, A. Nieto-Márquez, E. Alonso, Appl. Catal. Gen. 529 (2017) 49–59.
[20] D.K. Mishra, J.-M. Lee, J.-S. Chang, J.-S. Hwang, Catal. Today 185 (2012) 104–108.
[21] D. Liu, D. Zemlyanov, T. Wu, R.J. Lobo-Lapidus, J.A. Dumesic, J.T. Miller, C. L. Marshall, J. Catal. 299 (2013) 336–345.
[22] H. Li, D. Chu, J. Liu, M. Qiao, W. Dai, H. Li, Adv. Synth. Catal. 350 (2008) 829–836.
[23] H. Li, Y. Wang, Q. Zhao, H. Li, Res. Chem. Intermed. 35 (2009) 779–790.
[24] V.A. Sifontes Herrera, O. Oladele, K. Kordás, K. Eränen, J.-P. Mikkola, D. Yu. Murzin, T. Salmi, J. Chem. Technol. Biotechnol. 86 (2011) 658–668.
[25] V.A. Sifontes, D. Rivero, J.P. Wärnå, J.-P. Mikkola, T.O. Salmi, Top. Catal. 53 (2010) 1278–1281.
[26] E.M. Sulman, M.E. Grigorev, V. Yu. Doluda, J. Wärnå, V.G. Matveeva, T. Salmi, D. Yu. Murzin, Chem. Eng. J. 282 (2015) 37–44.
[27] M.L. Cunningham, C.B. Walker, 2004, US Patent 0224058.
[28] M. Niimi, Y. Hario, 1990, JP Patent 0342997.
[29] G. Garsow, 1991, EP Patent 423525.
[30] M. Magara, K. Shimazu, M. Fuse, 1989, JP Patent 0193597.
[31] R. Geyer, P. Kraak, A. Pachulski, R. Schödel, Chem. Ing. Tech. 84 (2012) 513–516.
[32] B. Hoffer, Appl. Catal. Gen. 253 (2003) 437–452.
[33] J.-P. Mikkola, R. Sjöholm, T. Salmi, P. Mäki-Arvela, Catal. Today 48 (1999) 73–81.
[34] S. Yamaguchi, S. Fujita, K. Nakajima, S. Yamazoe, J. Yamasaki, T. Mizugaki, T. Mitsudome, ACS Sustain. Chem. Eng. 9 (2021) 6347–6354.
[35] Y. Yong, G. Huajun, Z. Qingxiao, Z. Fang, L. Hui, Catal. Today 365 (2021) 282–290.
[36] Y. Yang, H. Gu, Q. Zhang, H. Li, H. Li, ACS Appl. Mater. Interfaces 12 (2020) 26101–26112.
[37] A. Sadier, D. Shi, A.-S. Mamede, S. Paul, E. Marceau, R. Wojcieszak, Appl. Catal. B Environ. 298 (2021), 120564.
[38] G. Chieffi, C. Giordano, M. Antonietti, D. Esposito, J. Mater. Chem. A 2 (2014) 11591–11596.
[39] Y. Fu, L. Ding, M.L. Singleton, H. Idrissi, S. Hermans, Appl. Catal. B Environ. 288 (2021), 119997.
[40] D. Shi, Q. Yang, C. Peterson, A.-F. Lamic-Humblot, J.-S. Girardon, A. Griboval-Constant, L. Stievano, M.T. Sougrati, V. Briois, P.A.J. Bagot, R. Wojcieszak, S. Paul, E. Marceau, Catal. Today 334 (2019) 162–172.
[41] J.-P. Mikkola, H. Vainio, T. Salmi, R. Sjöholm, T. Ollonqvist, J. Väyrynen, Appl. Catal. Gen. 196 (2000) 143–155.
[42] T.N. Pham, A. Samikannu, A.-R. Rautio, K.L. Juhasz, Z. Konya, J. Wärnå, K. Kordas, J.-P. Mikkola, Top. Catal. 59 (2016) 1165–1177.
[43] V.A. Sifontes Herrera, O. Oladele, K. Kordás, K. Eränen, J.-P. Mikkola, D. Yu. Murzin, T. Salmi, J. Chem. Technol. Biotechnol. 86 (2011) 658–668.